Bulgarian Chemical Communications, Volume 49, Special Issue A (pp. 59–70) 2017

Powder XRD microstructural analysis of thermally treated synthetic fluor-hydroxylapatite

V. V. Kostov-Kytin[1]*, V. Petkova[1,2], T. Kaljuvee[3]

[1] *Bulgarian Academy of Sciences, Institute of Mineralogy and Crystallography, 1113 Sofia, Acad. Georgi Bonchev Str., Bl. 107, Bulgaria*
[2] *New Bulgarian University, Department of Natural Sciences, 21 Montevideo Str., 1618 Sofia, Bulgaria*
[3] *Tallinn University of Technology, Lab. of Inorg. Materials, Ehitajate tee 5, 19086, Tallinn, Estonia*

Received October, 2016; Revised December, 2016

Samples of nano-sized synthetic Fluor-hydroxylapatite (SFHA) heated within the temperature range 400–910 °C are studied by powder X-ray diffraction (PXRD) analysis. Description of the microstructural characteristics at different temperatures as well as their evolution during the thermal treatment is in the focus of the investigations. The analysis of diffraction-line broadening is performed using Rietved refinement and applying various size and strain models to handle the distinct anisotropy observed in certain crystallographic directions. Trends and consistencies of patterns in terms of domain sizes and microstrain have emerged for the studied material upon heating. The obtained results are explained and interpreted in the light of the up-to-date views and theories on crystal growth and imperfections and modern PXRD microstructural approaches.

Keywords: apatite, Rietveld refinement, microstructural analysis, crystal growth.

INTRODUCTION

Apatite is the name of a group of phosphate minerals, usually referring to hydroxylapatite – $Ca_{10}(PO_4)_6(OH)_2$, fluorapatite – $Ca_{10}(PO_4)_6(F)_2$, and chlorapatite $Ca_{10}(PO_4)_6(Cl)_2$ [1]. As a major source of phosphorus for the plants its primary use is in the manufacture of fertilizer for the purposes of agriculture. Synthetic hydroxylapatite and fluorapatite have been extensively used as a bone implant material, because of its similarity with human bone composition and ability to form strong bond to the human hard tissue. Prior to bringing into use both natural and synthetic representatives of these materials are frequently subjected to various procedures like mechanoactivation and heating in order to improve their functionality and properties. Numerous investigations have contributed to obtain better knowledge about the apatite crystal structure, its compositional diversity and thermal stability [2, 3]. The following structural and physicochemical features of this material are of interest for the present study: i) the apatite structure can be presented as sheets lying in the (001) plane and comprising approximate hexagonally packed spheres each one represented by a tetrahedral PO_4^{3-} ion and containing also two different sized holes, the larger ones, where Ca^{2+}, reside being midway between the sheets [3]; ii) like all phosphate compounds, apatite refers to the anisodesmic compounds, which is a prerequisite for the emergence of zones of weak bonding along certain crystallographic planes and directions; iii) the apatite structure is known to manifest weak and imperfect cleavage along {001} and {100}.

Unlike the structural and macro-structural characterization of apatite less attention has been paid to the description and quantification of its microstructural parameters like crystallite size and various lattice imperfections for better understanding this material evolution upon various treatments in the nanoscale range.

Powder X-ray diffraction (PXRD) has actively come into use for the purposes of microstructural analysis during the last decades. An intrinsic feature of the XRD line profile analysis originating from its physical grounds is that it gives information for the bulk properties of a powder or a polycrystalline solid. When the PXRD data are processed by a software package involving the facilities of Rietveld refinement the obtained results provide information as

* To whom all correspondence should be sent:
E-mail: vkytin@abv.bg

for the crystal-chemical changes, phase transitions, and quantity of phases as well as for certain microstructural characteristics of the investigated crystalline matter like the coherently diffracting domain sizes and the microstrains distribution. Although the inspection of the line broadening is not yet a standard and universally adopted procedure, various size and strain models can be tested including also anisotropy of the microstructural distribution in terms of the reciprocal lattice vectors.

Apatite microstructural characteristics have already been object of investigation by local methods and PXRD.

Studying the effects of nanoindentation on natural and synthetic apatite crystals Chaikina has summarized that the greatest concentration of dislocation sites marked by the amount of etch pits as manifestation of their outlet is on the faces of dipyramides {10–11} and prism {10–10) [4]. Only isotropic, predominantly structureless size and strain models have been applied in the majority of works where PXRD analysis is applied to study the microstructural characteristics of apatite [5–8]. In their work Lala et al. [9] have focused attention on the pertinent explanation of the crystal growth mechanism of β-TCP on the account of nanocrystalline hydroxyapatite (HAp) upon its sintering to 1000 °C. They have also provided data for the anisotropy of the size and strain characteristics. Certain contradictions however emerge between the illustrative material presented by these authors and the interpretation of the obtained results e.g. their statement that "The maximum particle size is found along the plane (002) which is exactly perpendicular to c axis. Whereas, the planes parallel to c-axis have small particle sizes indicating the hindrance of growth of such planes parallel to c-axis" vs. the evidenced by the HRTEM images of a nano-sized HAp single crystal elongation along [002] in Fig 7b (inset) and data in Table 1 [9].

A well-known fact for the specialists in materials science is that heat treatment alters the physical properties of a material and is often accompanied by decrease of strain and stress in terms of various kinds of point, linear, and plane defects and increase of crystallite size. First attempts in terms of XRD to develop a phenomenological line-broadening theory were made referring to plastically deformed metals and alloys [10, 11]. The theory identifies two main types of diffraction line broadening: the size and strain components. The former depends on the size of coherent domains, which is not limited to the grains but may include effects of stacking and twin faults and small-angle boundaries caused by any lattice imperfection (dislocations and different point defects). The theory is general and was successfully applied to other materials, including oxides and polymers. In 2008, T. Ungár [12] has presented the dislocation model of strain anisotropy postulating that strain broadening can only be caused by dislocation-type lattice defects. On the other hand, from the theories of crystal growth it is known that the growth rate of the entire face is determined by the driving force at the point of emergence of the predominant point of growth (e.g. a dislocation, a foreign particle, or crystal twin) [13]. Thus, the dislocations spatial distribution and migration ability on the account of atomic bonds rearrangement that may occur upon heating of a crystalline material is closely related and can provoke crystal growth in certain crystallographic directions.

This study presents results from the microstructural characterization of nanosized synthetic Fluor-Hydroxylapatite performed using the facilities of the FullProf (FP) program [14] on collected PXRD patterns of samples heated within the temperature range 400–910 °C. Isotropic and various anisotropic size and strain models have been applied in order to achieve best whole profile fitting (WPF). Crystal-chemical control has been hold in all stages of the refinement. Certain trends and consistencies of patterns in terms of domain sizes and microstrain anisotropic appearance have emerged for the studied material upon heating and explanation for them is suggested in the light of the existing theories and models for crystal growth and deformations.

EXPERIMENTAL

Synthesis

Synthetic Fluor-HydroxylApatite (SFHA) was synthesized using a procedure reported by Nathanael *et al*., (2013) with only minor variations [15]. Calcium nitrate ($Ca(NO_3)_2.4H_2O$) and ammonium dihydrogen phosphate ($(NH_4)H_2PO_4$) instead of ($(NH_4)_2HPO_4$) were used as calcium (Ca) and phosphate (P) sources, respectively. Both sources mixed separately with distilled water were prepared in a way as to maintain the overall Ca/P ratio equal to 2. Ammoniumfluoride (NH_4F) was dissolved in water and added to the phosphate containing solution as a fluorine (F) source keeping the ratio P/F = 2. The pH of the phosphate containing solution was increased to 9 by adding ammonium hydroxide (30%). During the reaction the phosphate containing solution was added dropwise into the calcium containing solution with vigorous stirring for 1 h. The mixed solution was transferred to the Teflon beaker of the stainless steel autoclave and placed in the oven at 180 °C for 16 h. After the reaction the autoclave was cooled down to room temperature and the final precipitate was washed several times

with distilled water and ethanol and dried at 100 °C overnight.

Subsequently, portions of the as-synthesized material were heated in an oven at equal temperature intervals chosen in accordance with the TGA-DTG-DTA data up to 400 °C; 530 °C; 660 °C; 790 °C; and 910 °C, kept for 2 hours each one and cooled gradually to room temperature.

Analytical Procedure

Powder X-ray diffraction patterns of the samples were collected using a Bruker D2Phaser diffractometer with Ni-filtered CuKα radiation in the 2θ range from 5 to 70° and in a step-scan regime (step 0.015° and time 10 s per step). Thermogravimetric and differential thermal analyses (TGA-DTG-DTA) were performed on a SETSYS2400 thermal analyzer (SETARAM, France) in the temperature range 20–1200 °C, at a heating rate of 10 °C.min^{-1} in static air.

Structure and microstructural refinements

The theoretical XRD pattern has been simulated with Fluor-HydroxylApatite (FHA) (ICSD # 182890, hexagonal, S. G. P63/m, a = 9.3970 Å, c = 6.8820 Å) [16, 17].

The microstructural effects within FullProf [14] are treated using the Voigt approximation: both instrumental and sample intrinsic profiles are supposed to be described approximately by a convolution of Lorentzian and Gaussian components. The TCH pseudo-Voigt profile function is used to mimic the exact Voigt function. The integral breadth method to obtain volume averages of sizes and strains is used to output a microstructural file where an analysis of the size and strain contribution to each reflection is written if the user has provided an input file containing the instrumental resolution function (IRF) [18].

Initially, the crystal structures of the SFHA samples heated at different temperatures have been refined without applying any microstrucutral model just to confirm the materials phase purity and plausibility of the final crystal-chemical parameters. No substantial changes in the reflection positions or appearance of new ones have been detected and it is assumed that within the studied temperature interval the material has not undergone structural transformations or phase transitions. The profile parameters obtained for the sample heated to 910 °C have been incorporated in an IRF file that has later been used for the microstructural analysis.

Several isotropic size and strain models in terms of the Gaussian and Lorentzian components of the profile have been checked for each sample and the best results in terms of reliability factors and crystal-chemical plausibility are presented in the following section. Subsequently, the WPF continued with applying the General Size formulation model: Generalised size parameters (quadratic form) and preserved isotropicity of the Lorenzian strain model. Finally, pattern fitting has been performed using the Generalized Strain formulation model: Anisotropic Lorenzian Size Broadening Spherical Harmonics (SH) and Strain Broadening Model (quartic form). This actually presents a refinement procedure with simultaneous application of anisotropic size and anisotropic strain models in it. In all cases, the whole pattern fitting procedures have ended including in the refinement all those structural and profile parameters that would allow checking the plausibility of the obtained crystal-chemical characteristics.

RESULTS

Figure 1 gives notion about certain crystallographic planes and directions in apatite crystals being of interest for this study. Figure 2 demonstrates the anisotropy of line broadening, as well as the advantages of the anisotropic model used as compared with the isotropic one in the WPF procedure. Table 1 presents selected structural parameters of the studied samples obtained according to the applied refinement procedure and size and strain models using FullProf. The standard deviations appearing in the global average apparent size and strain is calculated

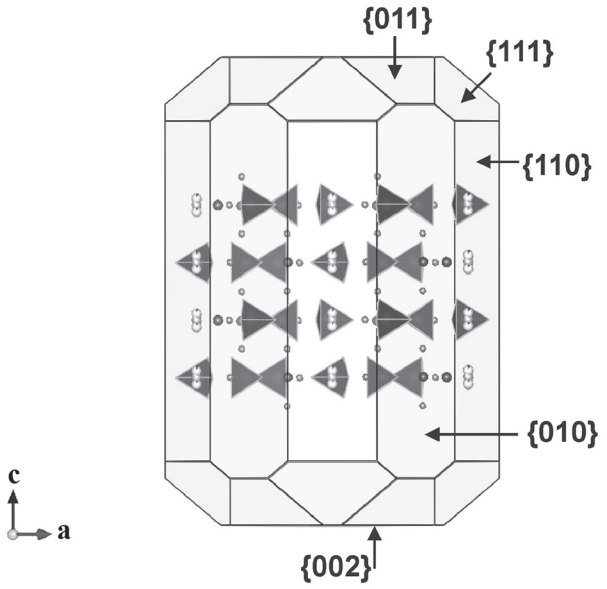

Fig. 1. Some of the most abundant forms of apatite crystals: pinacoid {002}; first-order prism {010}; second-order prism {110}; first-order dipyramid {011}; second-order dipyramid {111}.

Table 1. Selected structural parameters of the studied samples obtained according to the applied refinement procedure and size and strain models using FullProf (FP)

Samples of synthetic fluor-hydroxyl apatite (SFHA)					
As-synth	400 °C	530 °C	660 °C	790 °C	910 °C
FP pattern fitting without microstructural model – Standard approach					
$a = b$ = 9.3886(14) Å c = 6.8914(11) Å V = 526.1(1) Å^3 *ATZ= 1041.277	$a = b$ = 9.3750 (9) Å c = 6.8852 (7) Å V = 524.1(1) Å^3 ATZ= 1035.852	$a = b$ = 9.3670(6) c = 6.8872(5) V = 523.6(1) Å^3 ATZ= 1036.590	$a = b$ = 9.3703(4) Å c = 6.8849(3) Å V = 523.5(0) Å^3 ATZ= 1019.408	$a = b$ = 9.3705(3) Å c = 6.8850(2) Å V = 523.6(0) Å^3 ATZ= 1002.544	$a = b$ =9.3704(1) Å c = 6.8833(1) Å V = 523.4(0) Å^3 ATZ= 1003.352
χ^2 = 2.572 Rp = 17.3 Rwp = 21.9 Bragg R-factor = 4.99	χ^2 = 1.944 Rp = 15.1 Rwp = 17.9 Bragg R-factor = 3.07	χ^2 = 1.73 Rp = 14 Rwp = 16.7 Bragg R-factor = 2.89	χ^2 = 1.457 Rp = 12.7 Rwp = 15.3 Bragg R-factor = 2.51	χ^2 = 1.309 Rp = 11.5 Rwp = 14.3 Bragg R-factor = 2.81	χ^2 = 1.618 Rp = 12.5 Rwp = 15 Bragg R-f-r = 3.41
FP pattern fitting with Isotropic Lorenzian size (Å) and Lorenzian strain model (10^{-4})					
$a = b$ = 9.3902(5) Å c = 6.8927(4) Å V = 526.3(1) Å^3	$a = b$ = 9.3730(10) Å c = 6.8879(8) Å V = 524.1(1) Å^3	$a = b$ = 9.3697(3) Å c = 6.8872(2) Å V = 523.6(0) Å^3	$a = b$ = 9.3705(2) Å c = 6.8852(1) Å V = 523.6(0) Å^3	$a = b$ = 9.3705(3) Å c = 6.8852(2) Å V = 523.5(0) Å^3	$a = b$ =9.3703(1) Å c = 6.8830(1) Å V = 523.4(0) Å^3
χ^2 = 2.130 Rp = 16.1 Rwp = 19.3 Bragg R-factor = 3.84	χ^2 = 3.418 Rp = 18.5 Rwp = 22.5 Bragg R-factor = 4.38	χ^2 = 1.727 Rp = 14 Rwp = 16.6 Bragg R-factor = 2.92	χ^2 = 1.476 Rp = 12.7 Rwp = 15.2 Bragg R-factor = 2.52	χ^2 = 1.341 Rp = 11.6 Rwp = 14.4 Bragg R-factor = 2.93	χ^2 = 4.949 Rp = 22.7 Rwp = 25.8 Bragg R-f-r = 6.36
App. Size = 212.65 (0.25) Max Strain = 12.280 (0.0078)	App. Size = 145.86 (0.16) Max Strain = 41.473 (0.0494)	App. Size = 289.21 (0.20) Max Strain = 11.745 (0.0175)	App. Size = 456.42 (0.50) Max Strain = 7.2754 (0.0044)	App. Size = 790.93 (0.70) Max Strain = 8.7402 (0.0111)	App. Size = 2779.49 (2.92) ** Max Strain = 4.5818 (0.007) **

(Table 1 (continued)

FP pattern fitting with General size formulation Model (GSzfM): Generalised Size parameters (quadratic form), (Å)					
$a = b = 9.3898(3)$ Å $c = 6.8908(2)$ Å V = 526.2(0) Å^3	$a = b = 9.3748(3)$ Å $c = 6.8852(2)$ Å V = 524.0 (0) Å^3	$a = b = 9.3697(2)$ Å $c = 6.8868(2)$ Å V = 523.6(0) Å^3	$a = b = 9.3707(2)$ Å $c = 6.8852(1)$Å V = 523.6(0) Å^3	$a = b = 9.3705(1)$ Å $c = 6.8849(1)$ Å V = 523.6(0) Å^3	
$\chi^2 = 1.244$ Rp = 12.3 Rwp = 14.8 Bragg R-factor = 3.24	$\chi^2 = 1.265$ Rp = 12.0 Rwp = 14.5 Bragg R-factor = 3.45	$\chi^2 = 1.302$ Rp = 11.8 Rwp = 14.5 Bragg R-factor = 3.29	$\chi^2 = 1.252$ Rp = 11.3 Rwp = 14.0 Bragg R-factor = 2.91	$\chi^2 = 1.257$ Rp = 11.1 Rwp = 14.0 Bragg R-factor = 2.78	Resolution limited
Av. App. Size = 206.94 (77.28) and Table 2 Average max strain = 18.095 (0.0234)	Av. App. Size = 203.94 (58.66) and Table 2 Average max strain = 19.235 (0.0146)	Av. App. Size = 292.67 (70.12) and Table 2 Average max strain = 11.745 (0.0175)	Av. App. Size = 456.43 (80.97) and Table 2 Average max strain = 7.2754 (0.0044)	Av. App. Size = 859.00 (97.74) and Table 2 Average max strain = 8.7402 (0.0117)	
FP pattern fitting with the General Strain formulation Model: Anisotropic Lorenzian Size Broadening (SH), (Å) and Strain Broadening Model (Quartic form), (10^{-4})					
$a = b = 9.3895(3)$ Å $c = 6.8906(2)$ Å V=526.1(0) Å^3 ATZ= 1006.847	$a = b = 9.3743(3)$ Å $c = 6.8850(2)$ Å V = 524.0(0) Å^3 ATZ= 1006.667	$a = b = 9.3682(2)$ Å $c = 6.8856(2)$ Å V = 523.3(0) Å^3 ATZ= 1002.950	$a = b = 9.3707(2)$ Å $c = 6.8851(1)$ Å V = 523.6(0) Å^3 ATZ= 1005.880	$a = b = 9.3706(1)$ Å $c = 6.8849(1)$ Å V = 523.6(0) ATZ= 1003.204 Å^3	
$\chi^2 = 1.204$ Rp = 12 Rwp = 14.6 Bragg R-factor = 3.02	$\chi^2 = 1.233$ Rp = 11.8 Rwp = 14.4 Bragg R-factor = 3.25	$\chi^2 = 1.257$ Rp = 11.5 Rwp = 14.2 Bragg R-factor = 3.19	$\chi^2 = 1.209$ Rp = 11 Rwp = 13.8 Bragg R-factor = 2.87	$\chi^2 = 1.249$ Rp = 11 Rwp = 13.9 Bragg R-factor = 2.73	Resolution limited
Av. App. Size = 220.27 (64.98) and Table 3	Av. App. Size = 197.77 (43.53) and Table 3	Av. App. Size = 305.06 (32.28) and Table 3	Av. App. Size = 516.27 (82.07) and Table 3	Av. App. Size = 856.89 (90.73) and Table 3	
Av. max Strain = 29.5348 (11.7310) and Table 4	Av. max Strain = 24.5140 (7.9247) and Table 4	Av. max Strain = 20.4704 (5.0513) and Table 4	Av. max Strain = 14.1595 (3.0045) and Table 4	Av. max Strain = 8.4299 (0.5542) and Table 4	

*ATZ – Coefficient to calculate the weight percentage of the phase. ATZ = Z $M_w f^2$/ t (FullProf_Manual, [14])
**Data obtained when IRF file created with SiO_2 as a standard sample was used.

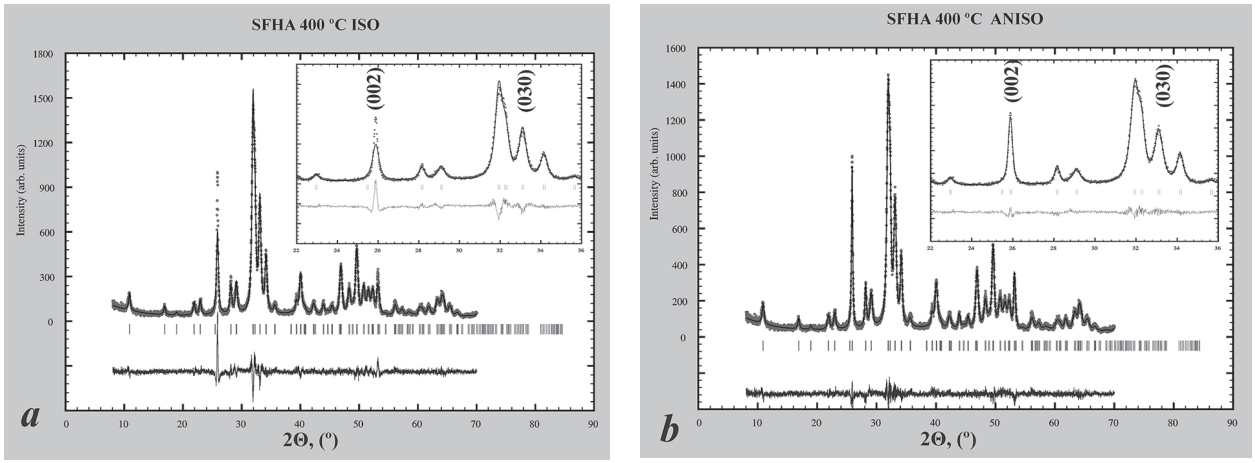

Fig. 2. Rietveld refinements for the SFHA sample heated at 400 °C: a) pattern fitting with isotropic Lorenzian size and Lorenzian strain model; b) pattern fitting with the Generalized Strain formulation model: Anisotropic Lorenzian Size Broadening (SH) and Strain Broadening Model (Quartic form). The circles are the experimental XRD data and the line through the markers is the result from the refinement. The Bragg positions are shown as short vertical lines. At the bottom is the difference plot between the data and the calculated profile.

using the different reciprocal lattice directions. It is a measure of the degree of anisotropy, not of the estimated error. Table 2 and Table 3 present apparent sizes along certain reciprocal lattice vectors according to the applied size and strain models, accordingly. Table 4 gives maximum strains values for selected crystallographic families after the corresponding refinement procedure has been used. Interestingly, when applying only the anisotropic Lorenzian size broadening (SH) for the sample heated to 530 °C FullProf refinement provides results for the (00*l*) reflections (data in bold in Table 3). However, when the anisotropic strain broadening model is included in the fitting procedure both size and strain results appear to be resolution limited (data in bold in Table 4). We do not have appropriate explanation for this. Figure 3 and Figure 4 present visualizations of the averaged crystallite shape and sizes obtained for the material heated to 660 °C (Table 3) and of the average maximum strain distribution tendencies

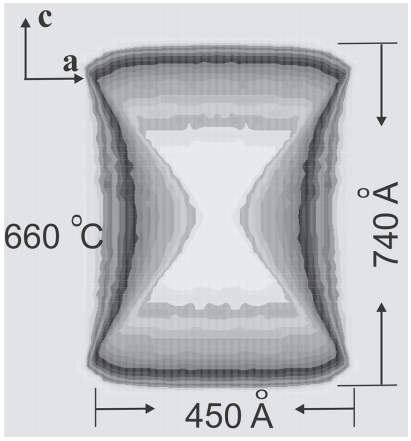

Fig. 3. Visualization of the average crystallite shape from refinement of the pattern with the Generalized Strain formulation model: Anisotropic Lorenzian Size Broadening (SH) and Strain Broadening Model (Quartic form) for the studied material heated to 660 °C as received by the GFOURIER module in FullProf.

Table 2. FullProf apparent sizes along selected Bragg reflections (*hkl*) (Å) of the studied samples after the General size formulation Model (GSzfM) was applied

	As-synth	400 °C	530 °C	660 °C	790 °C
(***0k0***)	159.91	171.31	248.14	398.10	781.63
(***0kk***)	211.03	208.33	300.11	491.98	901.47
(***hh0***)	171.21	179.86	253.55	401.49	820.98
(***hhh***)	190.64	188.85	284.16	438.31	852.21
(***00l***)	543.09	456.29	549.82	728.45	1168.56
(***00l***) / (***0k0***)	3.396	2.664	2.216	1.830	1.495

Table 3. Apparent sizes along selected Bragg reflections orders (*hkl*) after the General Strain formulation Model: Anisotropic Lorenzian Size Broadening (SH) and Strain Broadening Model (Quartic form) were applied in the FullProf refinement, (Å)

	As-synth	400 °C	530 °C	660 °C	790 °C
(*010*)	175.35	173.22	286.08	448.13	786.03
(*020*)	174.21	164.75	285.27	445.28	781.41
(*030*)	188.48	177.92	286.11	448.01	786.54
(*040*)	193.08	178.45	286.36	448.12	786.73
(*050*)	183.55	173.37	285.84	447.11	784.85
(*060*)	189.17	178.56	286.16	448.14	786.77
(0k0) averaged	183.97	174.38	285.97	447.47	785.39
(*011*)	237.00	208.62	339.12	541.51	880.56
(*022*)	237.00	208.62	339.12	541.51	880.56
(*033*)	223.01	197.35	338.40	539.07	876.63
(0kk) averaged	232.34	204.86	338.88	540.67	879.25
(*110*)	228.81	197.63	299.27	488.76	842.87
(*220*)	243.38	208.80	299.83	490.74	846.45
(*330*)	232.01	200.09	299.40	489.22	843.69
(hh0) averaged	234.73	202.17	299.5	489.58	844.34
(*111*)	217.12	192.01	303.14	500.41	836.59
(*222*)	212.48	188.26	302.92	499.62	835.24
(hhh) averaged	214.8	190.14	303.03	500.02	835.92
(*002*)	502.79	377.31	535.08	738.70	1118.60
(*004*)	502.79	377.31	535.08	738.70	1118.60
(00l) averaged	502.79	377.31	**535.08***	738.70	1118.60
averg. app. size, Å³, Table 1	220.27 (64.98)	197.77 (43.53)	305.06 (32.28)	516.27 (82.07)	856.89 (90.73)
(00l) averaged / (0k0) averaged	2.87	2.16	1.75	1.65	1.42

* see RESULTS

Table 4. Maximum-strains for selected crystallographic families {hkl} after the General Strain formulation Model: Anisotropic Lorenzian Size Broadening (SH) and Strain Broadening Model (Quartic form) were applied in the FullProf refinement, (10^{-4})

	As-synth	400 °C	530 °C	660 °C	790 °C
{0k0}	41.1863	33.2999	25.2034	17.2382	9.0697
{0kk}	12.2812	15.2440	11.7062	11.2760	7.8054
{hh0}	41.1863	33.2999	25.2034	17.2382	9.0697
{hhh}	25.7652	22.7116	18.2267	13.9017	8.2619
{00l}	10.2422	13.4004	**res. lim.***	7.9346	7.5815
av. max Strain	29.5348 (11.7310)	24.5140 (7.9247)	20.4704 (5.0513)	14.1595 (3.0045)	8.4299 (0.5542)

* see RESULTS

upon heating (Table 4), respectively. Figure 5 is a schematic presentation of the average for all crystalline domains apparent sizes at a particular temperature, scaled along the normal to the scattering planes (0*k*0) and (00*l*). Table 5 contains selected interatomic distances for the coordination polyhedra in SFHA material at different temperatures upon applying the simultaneous anisotropic size and strain refinement procedure. Obviously, all obtained results concerning the size and strain characteristics of the studied samples are model-dependent (Tables 1–3). Despite some differences in the magnitudes of the refined parameters a clear tendency is observed in the behavior of the title material upon heating and namely – crystal domain enlargement and microstrain diminishment with the increase of temperature. Some deviations from this trend within the interval around 400–550 °C are accompanied by

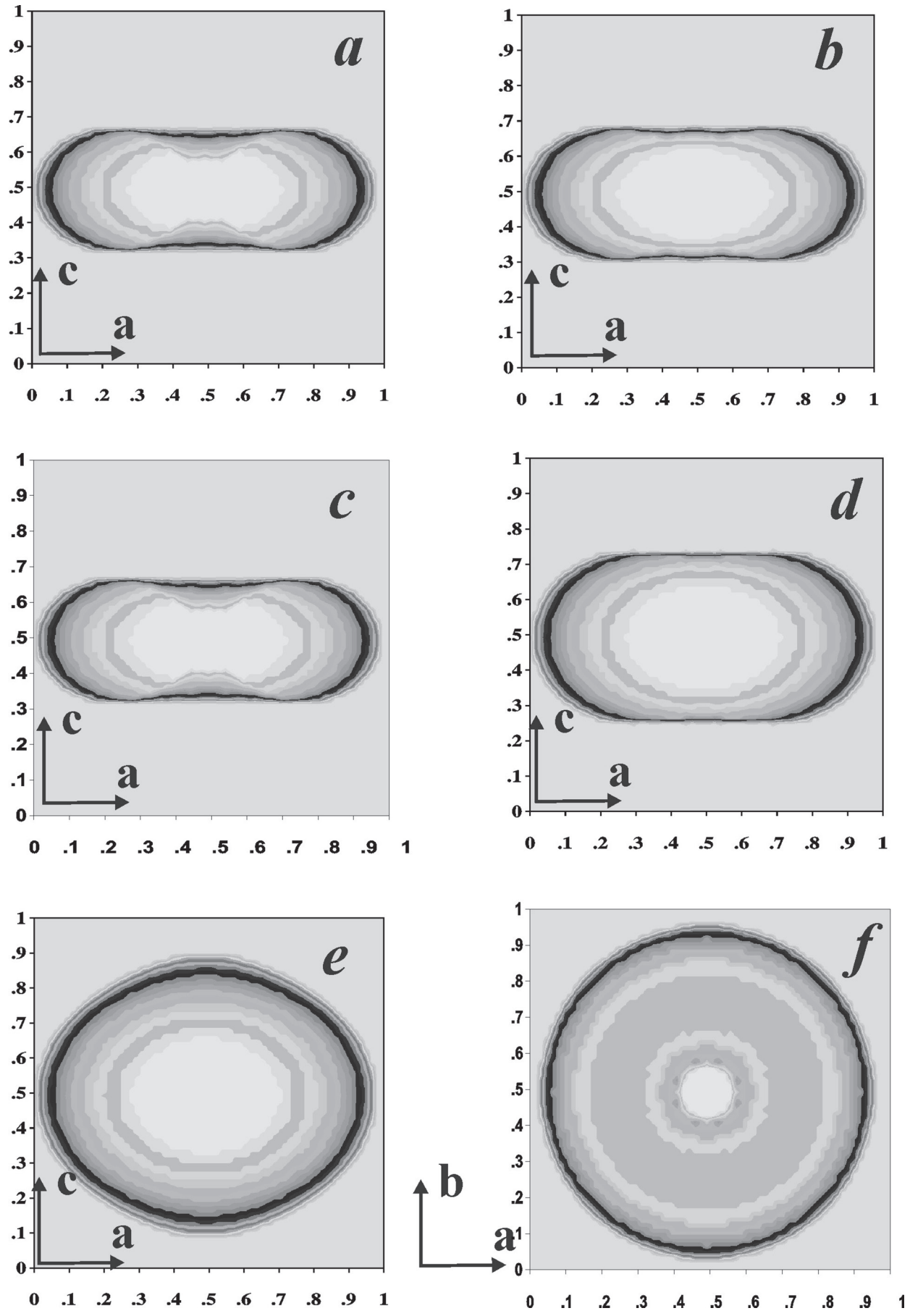
a
b
c
d
e
f
c
a
b
0 .1 .2 .3 .4 .5 .6 .7 .8 .9 1

←

Fig. 4. Visualization of the average maximum strain from refinement of the patterns with the Generalized Strain formulation model: Anisotropic Lorenzian Size Broadening (SH) and Strain Broadening Model (Quartic form) for the studied material: a) as-synthesized; b) 400 °C; c) 530 °C, d) 660 °C, e) 790 °C, and f) strain in the **ab** plane equal for all samples as received by the GFOURIER module in FullProf.

Table 5. Selected interatomic distances (Å) for the coordination polyhedra in SFHA material at different temperatures after the General Strain formulation Model: Anisotropic Lorenzian Size Broadening (SH) and Strain Broadening Model (Quartic form) were applied in the FullProf refinement, (Å)

	As-synth	400 °C	530 °C	660 °C	790 °C
Ca1O9 polyhedron					
Ca1 – O1 x 3	2.411(6)	2.425(7)	2.420(7)	2.399(6)	2.402(5)
Ca1 – O2 x 3	2.443(7)	2.429(7)	2.430(6)	2.450(5)	2.448(5)
Ca1 – O3 x 3	2.832(5)	2.836(6)	2.826(4)	2.824(4)	2.827(4)
Ca2O6F polyhedron					
Ca2 – O1 x 1	2.701(9)	2.656(9)	2.684(8)	2.680(7)	2.682(5)
Ca2 – O2 x 1	2.397(9)	2.407(9)	2.406(7)	2.386(6)	2.377(6)
Ca2 – O3 x 2	2.500(6)	2.526(7)	2.501(5)	2.489(5)	2.483(4)
Ca2 – O3 x 2	2.321(5)	2.306(5)	2.318(4)	2.333(4)	2.344(4)
Ca2 – (O4,F) x 1	2.309(4)	2.301(4)	2.295(3)	2.302(3)	2.303(2)
PO4 tetrahedron					
P – O1	1.510(11)	1.501(12)	1.497(10)	1.529(9)	1.528(7)
P – O2	1.542(9)	1.540(9)	1.530(8)	1.526(7)	1.533(6)
P – O3	1.559(5)	1.559(5)	1.562(4)	1.551(4)	1.540(4)
P – O4	1.559(5)	1.559(5)	1.562(4)	1.551(4)	1.540(4)
max Δ(cc-l)*	0.049	0.058	0.065	0.022	0.012

* see DISCUSSION

weight loss registered in the TG-DTG-DTA curves for the as-synthesized sample (Fig. 6) and are discussed in the following section.

DISCUSSION

In this work the microstrain presence and orientation are accepted as almost entirely being due to the availability and the spatial distribution of dislocation defects. The dislocation density is strongly influenced by symmetrical and physicochemical considerations peculiar for the studied material (space group requirements and zones of weak atom bonding due to anisodesmicity). Thermal treatment facilitates the dislocations ability to migrate as a rule within the plane aligned by their directions and their Burgers vectors. The occurring upon this process atomic bonds rearrangement provokes atomic ordering in certain crystallographic directions and corresponding spatial increase of the coherently diffracting domains.

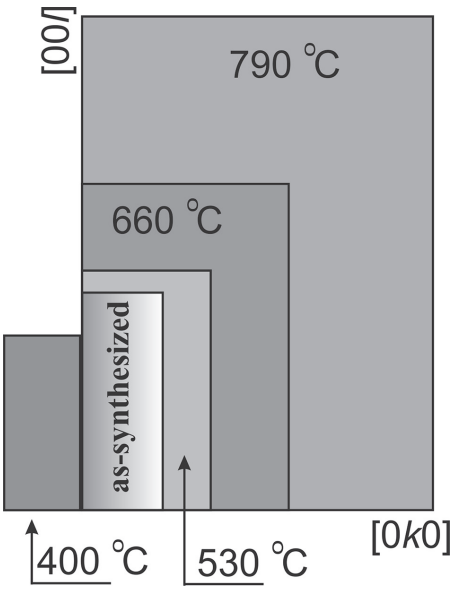

Fig. 5. Schematic presentation of the average for all crystalline domains apparent sizes at a particular temperature scaled along the normal to the scattering planes (0*k*0) and (00*l*).

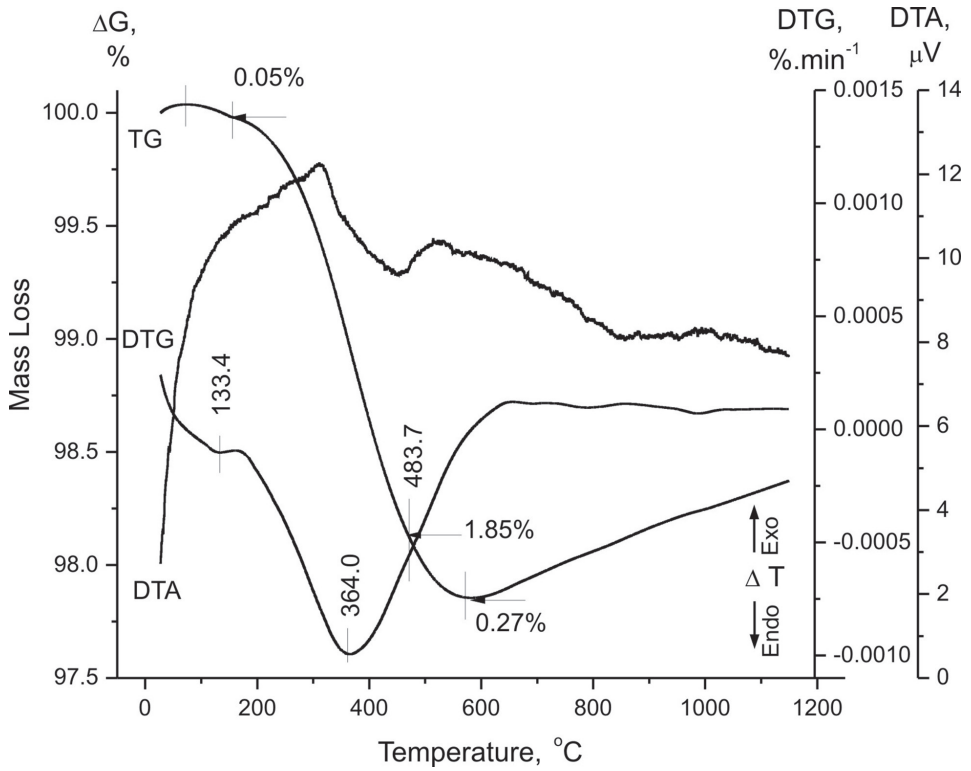

Fig. 6. TG-DTG-DTA curves of as-synthesized SFHA.

Indeed, such assumptions find evidence in the presented illustrative material (Fig. 3, 4; Tables 3, 4). Both size and strain manifest anisotropic distributions. The longest dimensions (41.186 10^{-4}, Table 4) of the initial almost disk-shaped form of the average maximum strain obtained for the as-synthesized SFHA lie in the crystallographically most symmetrical a-b plane (Fig.4 a, f) and parallel to the indistinct cleavage reported for the {001} crystal form. In contrast, the strain magnitude along the *c*-axis is nearly four times smaller (10.242, Table 4). Upon heating, maximum strains tend to diminish in all directions; however the process goes faster in the **ab** plane (Table 4). Figure 4e depicts almost isotropic dislocation distribution for the sample heated to 790 °C. Although the average crystallite shape manifests opposite to the strain distribution form (Table 3 and Fig. 3) its thermal evolution in terms of domain sizes in certain crystallographic directions is similar to that one observed for the strain. Thus domains increase more rapidly along [100] and [110] and less pronouncedly along [001] facilitated by the "healing" effect of the heating over the migration and cancellation of the dislocations in those directions. In other words the initial long prismatic crystallites turn into short-prismatic ones at the end of the process (Table 3, Fig. 5).

Some deviations from this trends are registered in the temperature interval around 400–530 °C. Certain decrease of domain size for the sample heated to 400 °C is obtained (Table 3, Fig. 4c). Overall decrease of the average maximum strain is observed when a refinement procedure with simultaneous application of anisotropic size and anisotropic strain models is applied however this is not the case when other refinements models have been used (Table 1 and Table 4). Besides, relative strain increase is detected along [001] and some other directions for the sample heated to 400 °C. A plausible explanation for this can be the fact that being a product of wet chemistry SFHA has comprised in its structure an extra amount of hydroxyl groups. Within the mentioned temperature interval their motion and rearrangement is provoked and they start to act like additional (point or line) defects, simultaneously hampering the migration of the existing dislocations and causing their spatial ordering possibly into arrays within the weak bonding zones. It is suggested now that for a while by causing slight misorientations within the crystalline domains these arrays play the role of small-angle grain boundaries that cause splitting and subsequent size decrease as registered by FullProf. Upon temperature increase a dehydroxylation occurs as evidenced by the mass

loss of 2.12% which equals the amount of approximately one molecule of water per unit cell (Fig. 6). After its liberation the crystalline material continues its evolution in the common pathway by size increase and microstrain diminishment. Additional facts supporting this suggestion are the ATZ values obtained from the whole pattern fitting without applying any microstructural model (Table 1) and the degree of the phosphorous coordination polyhedron distortion in terms of the maximal difference of the bond lengths central cation-ligand established for each temperature (max Δ(cc-l), Table 5).

CONCLUSIONS

The performed PXRD microstructural analysis reveals distinct anisotropy in the patterns line-broadening of nano-sized SFHA samples heated within the temperature range 400–910 °C. Profile broadening is caused as from the presence of nano-sized crystalline domains as well as from the occurring microstructural effects.

Both microstructural characteristics manifest opposite trends in their evolution upon thermal treatment. Whereas, in general, size tends to increase most pronouncedly along [110] and [010] (4-fold) and to a less extend along [001] (2-fold), strain diminishes with similar in intensity and directions manner until reaching a nearly isotropic spatial distribution. The deviation from this pathway between *ca*. 400–550 °C is explained with atomic rearrangements and mass-loss of nearly one H_2O molecule per formula unit.

Assuming that microstrain effect is due mainly to the presence of dislocations and dislocation-type defects a plausible explanation can be found for the interrelated behavior of size and strain parameters in the light of the up-to-date views for crystal growth and imperfections. Heating provokes dislocations migration and cancelation preferably within zones of weak atomic bonding. This process is accompanied by crystal growth occurring in the corresponding directions. For apatites such zones appear to coincide with the **ab** crystallographic planes in which the indistinct cleavage {001} has also been observed for this material.

This study provides a reliable and easy to apply approach for specialists in materials science to investigate through PXRD the bulk properties of a powder or a polycrystalline solid in terms of their microstructural characteristics.

Acknowledgments: *This work was supported by a bilateral contract category 'a' between the Bulgarian and Estonian Academies of Sciences. The financial support of the Department of Natural Sciences, the Gemology Laboratory – BF, and the Chemistry Laboratory of the New Bulgarian University is also acknowledged.*

REFERENCES

1. The New IMA (International Mineralogical Association) List of Minerals – A Work in Progress – Updated: July 2016 - http://nrmima.nrm.se//IMA_Master_List _%282016-07%29.pdf
2. J. C. Elliott, Structure and Chemistry of the Apatites and Other Calcium Orthophosphates (Studies in Inorganic Chemistry, vol. 18), Elsevier, Amsterdam-London-New York-Tokyo, 1994.
3. J. C. Elliott, R. M. Wilson and S. Dowker, Apatite structures, JCPDS-International Centre for Diffraction Data 2002, Advances in X-ray Analysis, Volume 45, 2002.
4. M. V. Chaikina, Mechanochemistry of Natural and Synthetic Apatites, Novosibirsk Publishing House of SB RAS, Branch "Geo", 2002 (in Russian).
5. A. A. Baig, J. L. Fox, R. A. Young, Z. Wang, J. Hsu, W. I. Higuchi, A. Chhettry, H. Zhuang, M. Otsuka, *Calcif Tissue Int*, **64**, 437 (1999).
6. K. Venkateswarlu, A. Chandra Bose, N. Rameshbabu, *Physica B* **405**, 4256 (2010).
7. K.D. Rogers, P. Daniels, *Biomaterials* **23**, 2577 (2002).
8. K. Venkateswarlu, D. Sreekanth, M. Sandhyarani, V. Muthupandi, A. C. Bose, and N. Rameshbabu, *International Journal of Bioscience, Biochemistry and Bioinformatics*, **2**, **6**, (2012).
9. S. Lala, B. Satpati, S.K. Pradhan, *Ceramics International*, **42**, 13176 (2016).
10. B. E. Warren, *Progr. Metal Phys*., **8**, 147 (1959).
11. B. E. Warren, B. L. J. Averbach, *Appl. Phys*., 21, 595 (1950).
12. T. Ungár, Dislocation Model of Strain Anisotropy, JCPDS-International Centre for Diffraction Data, 2008.
13. Frank, F. C. *Discussions of the Faraday Society*. **5**, 48 (1949).
14. J.R. Carjaval, *Physica B*, **192**, 55, (1993).
15. A. J. Nathanael, D. Mangalaraj, S. I. Hong, Y. Masuda, Y.H. Rhee, H. W. Kim, Materials Chemistry and Physics, 137, 3, 967 (2013).
16. Inorganic Crystal Structure Database (ICSD), Karlsruhe: Gmelin institute fur anorganische Chemie, 2005.
17. M. Rossi, M. R.Ghiara, G.Chita, F.Capitelli, American Mineralogist, 96, 1828 (2011).
18. J. R. Carvajal, Study of Micro-Structural Effects by Powder Diffraction Using the Program FULLPROF, https://www.ill.eu/fileadmin/users_files/documents/news_and_events/workshops_events/2015/FP School- 015/Microstructural_effects_FP.pdf.

ПРАХОВ РЕНТГЕНО-ДИФРАКЦИОНЕН МИКРОСТРУКТУРЕН АНАЛИЗ НА ТЕРМИЧНО ОБРАБОТЕН СИНТЕТИЧЕН ФЛУОР-ХИДРОКСИЛ АПАТИТ

В. В. Костов-Китин[1]*, В. Петкова[1,2], Т. Калюжий[3]

[1] Институт по минералогия и кристалография „Акад. Ив. Костов“, Българска академия на науките, София 1113, ул. Акад. Г. Бончев, бл. 107, България
[2] Нов Български Университет, Факултет Природни Науки, София 1618, ул. Монтевидео 21, България
[3] Талински Технологичен Университет, Лаборатория по Неорганични Материали, Ehitajate tee 5, 19086, Талин, Естония

Постъпила октомври, 2016 г.; приета декември, 2016 г.

(Резюме)

Образци от нано-размерен флуор-хидроксил апатит, отгрявани в температурния интервал 400–910 °C са изучавани чрез прахов рентгено-дифракционен анализ. Във фокуса на изследванията са описание на микроструктурните характеристики при различни температури, както и тяхното развитие по време на термичната обработка. Анализът на профилните уширения на дифракционната линия е осъществен чрез метода на Ритвелд, като са прилагани различни модели за размерност и напрежение при третирането на отчетливата анизотропност, наблюдавана в определени кристалографски направления. При нагряването се проявяват тенденции и закономерности по отношение на големината на кристалните домени и микронапреженията в изучавания материал. Получените резултати са обяснени и интерпретирани съгласно сега съществуващите възгледи и теории за кристален растеж и дефектност на структурата и в светлината на модерните разбирания за прахов рентгено-дифракционен микроструктурен анализ.